

Thermal kinetic and dielectric parameters of acenaphthene crystal grown by vertical Bridgman technique

S. Karuppusamy¹ · K. Dinesh Babu¹ · V. Nirmal Kumar^{1,2} · R. Gopalakrishnan¹

Received: 6 October 2015 / Accepted: 26 March 2016 / Published online: 11 April 2016
© Springer-Verlag Berlin Heidelberg 2016

Abstract The bulk acenaphthene crystal was grown in a single-wall ampoule by vertical Bridgman technique. X-ray diffraction analysis confirmed the orthorhombic crystal system of title compound with space group $Pcm2_1$. Thermal behavior of compound was studied using thermogravimetry—differential scanning calorimetry analysis. Thermal kinetic parameters like activation energy, frequency factor, Avrami exponent, reaction rate and degree of conversion were calculated using Kissingers and Ozawa methods under non-isothermal condition for acenaphthene crystal and reported for the first time. The calculated thermal kinetic parameters are presented. Dielectric studies were performed to calculate the dielectric parameters such as dielectric constant, dielectric loss, AC conductivity, and activation energy from Arrhenius plot.

1 Introduction

The growth of organic crystals by melt growth technique was investigated widely because of their potential applications in optical, electronic and optoelectronic devices [1–5]. For such applications the basic physical (optical transparency, electrical parameters, etc.) and chemical properties (structural, bonding nature, thermal stability, etc.) of the materials are to be studied well. Growth of crystals from melt involved the control over many parameters like, nucleation, temperature

gradient zone, temperature profile of the furnace, viscosity of liquid, thermal conductivity of the compound, meniscus shape of liquid–solid interface, growth rate and cooling rate. To grow defect free bulk single crystals, the above properties should be understood and optimized well [6–10]. Theoretical assumption and calculations were performed by several research groups for different kinds of materials to improve their crystalline perfection [11–14]. Mostly they have discussed thermal related properties (thermal conductivity, heat transfer, viscosity of liquid, etc.) of the material, furnace setup, effect of magnetic field on the material and heat flow in the melt.

The thermal parameters of materials play a vital role in formation of nucleation [15]. To study the thermal properties, it is very much important to understand the mechanism of nucleation in crystal growth process for a particular material which is considerably useful to grow defect free crystals from melt growth methods. By using Arrhenius equation, thermal kinetic parameters were calculated for many inorganic materials such as, hydrated iron sulfate [16], dolomite [17], molybdate(IV) and tungstate(IV) with chromium(III) [18] and cobalt sulfate hexahydrate [19]. Even though there are many studies and elucidations on organic crystals grown by melt technique and solution growth methods, no investigation reports on thermal kinetic parameters of organic crystal are available. The researchers have performed isothermal and non-isothermal studies for various materials, in which non-isothermal method is implemented for wide range of temperature in shorter time duration [20]. The thermal kinetic parameters were evaluated using Arrhenius equation and different types of equations were derived by different researchers like Kissingers, Ozawa, Augis and Bennet, Kissinger–Akahira–Sunose (KAS), and Ozawa–Flynn–Wall (OFW) [21–24].

✉ R. Gopalakrishnan
krgkrishnan@annauniv.edu; krgkrishnan@yahoo.com

¹ Crystal Research Laboratory, Department of Physics, Anna University, Chennai, India

² Research Institute of Electronics, Graduate School of Science and Technology, Shizuoka University, Hamamatsu, Japan

The acenaphthene crystal was grown by vertical Bridgman technique, and it was previously reported by Ramesh Babu et al. [25], using double-wall ampoule, and they have investigated some of the physical properties such as transmittance, nonlinear optical (NLO), etching, mechanical stability and then chemical parameters like structural analysis and thermal stability. The acenaphthene crystal has orthorhombic crystal system with space group $Pcm2_1$ [26]. The acenaphthene compound has low melting point and the compound is thermally stable up to its melting point. It does not have any phase changes before its solid to liquid phase transformation. In order to improve the optical and electrical properties for NLO and ferroelectric applications, the basic thermal kinetic parameters have to be determined for acenaphthene crystal. The main advantage of Bridgman technique is no need of seed crystal, here the seed crystal is formed at tip of ampoule which is due to the formation of nucleation where super-cooling occurs in the ampoule.

The acenaphthene bulk single crystal was successfully grown by vertical Bridgman technique at low temperature (97 °C) using single-wall ampoule with conical tip for the present investigation. Mainly, in this article, it is focused to understand the thermal kinetic parameters such as activation energy (E_a), frequency factor or pre-exponential factor (K_0), Avrami exponent (n), and reaction rate (K) from DSC curve using Kissinger's equation and also, degree of conversion (α) was evaluated from TG curve. The activation energy is calculated through Ozawa equation. From dielectric studies, dielectric constant, dielectric loss, AC conductivity, and activation energy of acenaphthene crystal were evaluated. Finally, the variation of activation energy due to thermal and electrical behavior of the grown organic crystal was evaluated.

2 Experiment

To grow the bulk acenaphthene crystal, homemade single-zone cylindrical furnace was used which is made up of borosilicate glass. We have slightly modified the previously constructed furnace to grow the acenaphthene crystal by using single-wall ampoule. Temperature of the furnace was measured by K-type thermocouple and the temperature profile of the furnace is shown in Fig. 1a. The borosilicate single-wall ampoule was prepared with the wall thickness of 1.2 mm to grow the bulk crystal. For design of ampoule, the dimensions, like inner diameter 10 mm, cone length 50 mm and length 150 mm, were used. The schematic diagram of the ampoule is shown in Fig. 1b. In order to remove the impurities inside the ampoule, it was cleaned with soap solution and thoroughly washed using double-

distilled water and subsequently rinsed with ethanol and then dried well at 80 °C.

2.1 Sample preparation

The polycrystalline material was obtained by slow evaporation solution growth technique using ethanol as a solvent. After attaining the supersaturated solution the solution was kept at room temperature, and it was allowed to evaporate. After a few days, a number of polycrystals were obtained, and good-quality crystals were chosen and ground well. Now, the powder sample was loaded into the ampoule.

2.2 Growth of acenaphthene crystal

The loaded ampoule (Fig. 1c) was evacuated to 10^{-4} Torr and sealed. Sealed ampoule was hanged using an aluminum wire into the furnace and lowered in temperature gradient. When the temperature reaches above the melting point of acenaphthene, the ampoule was maintained at same temperature for 4 h to completely melt the compound and to attain the homogeneity. After achieving equilibrium of liquid, the ampoule was allowed to move downward in the furnace at temperature gradient. Lowering the ampoule is controlled by a separate control system with the optimized lowering rate of 0.5 mm/h. While ampoule is moving downward, the nucleation is originated from minimum radius (tip) of the conical section at the ampoule as well as crystallization process continues. The grown crystal of bulk acenaphthene was harvested after 10 days, and it was cut for further studies (Fig. 1d). The surface of the harvested bulk acenaphthene crystal obtained was cleaned with double-distilled water.

2.3 Characterization studies

The structure of the title compound was confirmed by single crystal X-ray diffraction (XRD) analysis by using Bruker AXS Kappa APEX II single crystal X-ray diffractometer, the data were collected at room temperature and powder X-ray diffraction (XRD) analysis using BRUKER D2 PHASER. $CuK\alpha$ radiation (1.5418 Å) with scanning rate of 0.02° was used for measurement in the range 10° – 60° . The NMR spectral analysis was carried out by using BRUKER AVANCE III 500 MHz (AV 500) multi-nuclei solution NMR spectrometer. To know the thermal stability, phase transformation and kinetic parameters of obtained acenaphthene crystalline sample, thermogravimetry, and differential scanning calorimetry (TG–DSC) studies were carried out under nitrogen (N_2) atmosphere using NETZSCH STA 449F3 instruments. The thermogram was recorded from room temperature to 500 °C with various heating rates (β) like 5, 10, 15, 20 and 25 °C/min, and same sample mass was used for all the

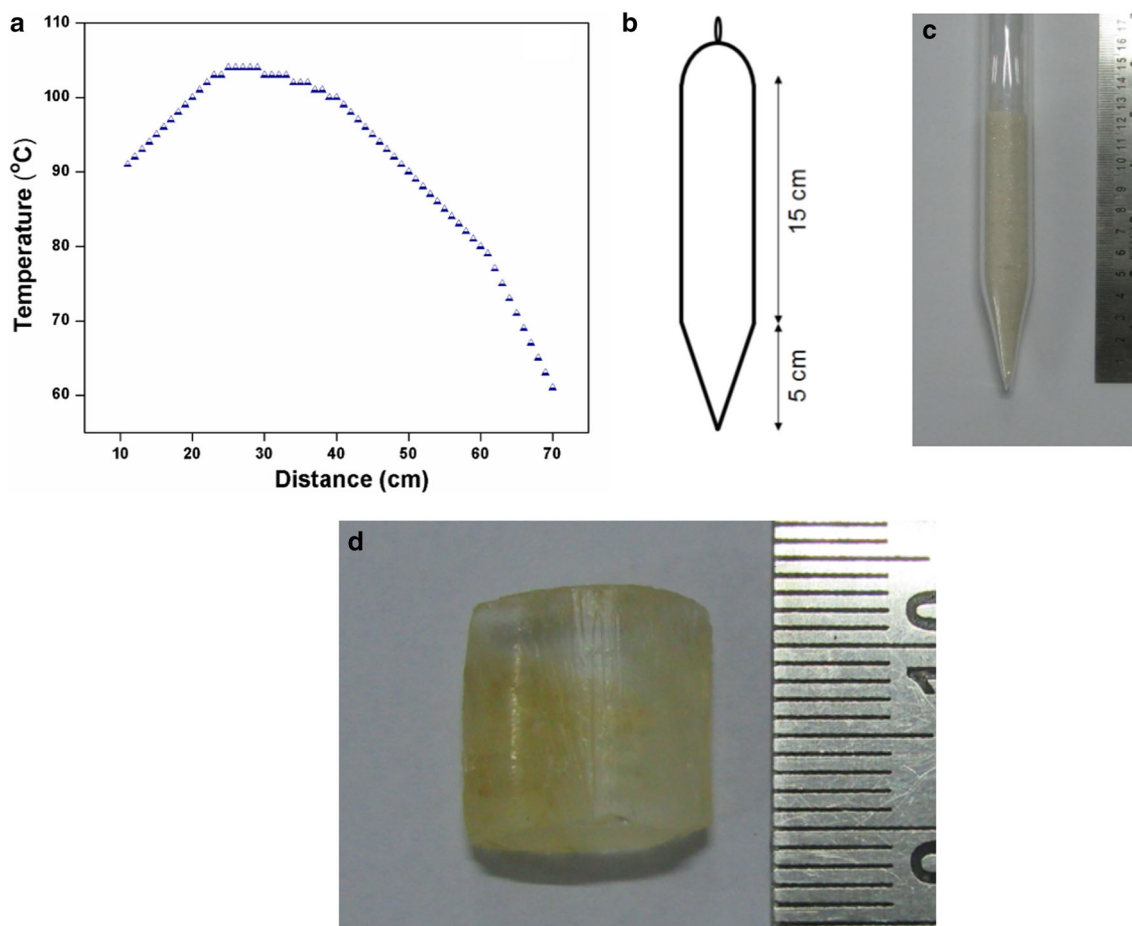


Fig. 1 **a** Temperature profile of the furnace, **b** borosilicate ampoule, **c** loaded ampoule, **d** acenaphthene crystal

experiments with different heating rate. The melting point of a particular material is varying due to change in mass and heating rate of the sample [27]. Good-quality crystal of acenaphthene with $\langle 020 \rangle$ orientation was selected for dielectric measurements using HIOKI 3532-50 LCR HITESTER with the selected dimension of $7.29 \times 5.31 \times 1.51 \text{ mm}^3$. The dielectric studies were carried out by forming a parallel-plate capacitor. The sample was coated with silver to obtain a good conductive surface layer which was placed between the two copper electrodes. The capacitance and dielectric loss were measured with the conventional parallel-plate capacitor method. The applied frequency varies from 50 Hz to 5 MHz, and the capacitance of the sample was noted at different temperatures like 40, 45, 50, 55, 60, and 65 °C.

3 Results and discussion

3.1 XRD analysis

From single crystal X-ray diffraction analysis, the acenaphthene crystal exhibits orthorhombic crystal system

Table 1 Lattice parameter values of acenaphthene

a (Å)	b (Å)	c (Å)	Reference
8.292	14.011	7.215	[25]
8.290	14.000	7.225	[26]
8.303	14.029	7.236	PXRD
8.306	14.011	7.274	Single crystal XRD

with space group of $Pcm2_1$. Obtained lattice parameter values are presented in Table 1. Powder XRD pattern of acenaphthene was indexed with Powder-X software package as shown in Fig. 2 and matched with the reported values (JCPDS card number: 32-1501). The calculated lattice parameters are presented in Table 1.

In previously reported [26] data, they have carried out structure refinement for acenaphthene crystal with more number of reflection data. But, in our case we have measured only for a few reflection data to identify the lattice parameter values to confirm the crystal structure. More accurate reflection data will yield highly perfect lattice

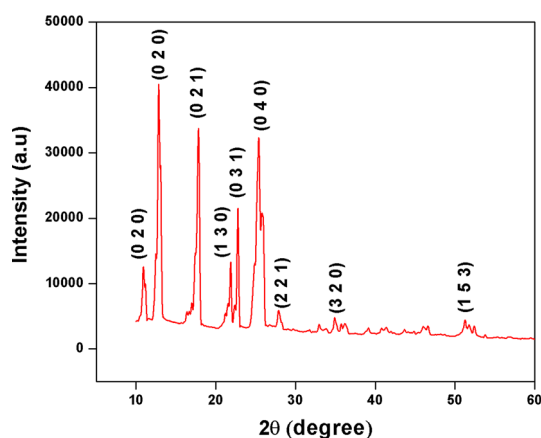


Fig. 2 X-ray diffraction pattern of acenaphthene

parameter values. While growing the crystal at different atmosphere or solvent, the size of unit cell may slightly increase or decrease due to lattice distortion. Hence, we got slight variation in lattice parameter values.

3.2 ^1H NMR analysis

The ^1H NMR analysis was carried out to further confirm the grown acenaphthene compound, and the recorded spectrum is shown in Fig. 3. The spectrum shows two doublet peak at $\delta = 7.55$ ppm and $\delta = 7.24$ ppm and one triplet peak at $\delta = 7.40$ ppm, which confirms the three different types of aromatic protons present in title compound. The singlet peak observed at $\delta = 3.34$ ppm represents the presence of four protons in two methylene groups at same environment of acenaphthene compound.

3.3 Determination of thermal kinetic parameters

The TG–DSC curves recorded at the heating rate of $10\text{ }^\circ\text{C}$ are shown in Fig. 4 which showed the material is stable up to $91\text{ }^\circ\text{C}$. The DSC curve had two sharp peaks at 96 and $220\text{ }^\circ\text{C}$ which revealed the melting point and decomposition point of the acenaphthene crystal. The melting point of the present material is slightly higher than that of previously reported one, owing to removal of impurities by repeated recrystallization process. It was observed that there is no phase conversion before solid–liquid transformation of acenaphthene. The thermal kinetics of a material can be estimated from TG, DTA and DSC techniques. The isothermal kinetics of material were based on Jhonson–Mehl–Avrami (JMA) equation, but in DSC technique both isothermal and non-isothermal cases can be used [28, 29].

To determine the reaction rate and thermal kinetics, Kissingers method and Ozawa method were used. From the peaks of DSC curve, the thermal kinetics were examined

under non-isothermal conditions in nitrogen (N_2) atmosphere for acenaphthene crystal.

The basic Avrami equation [29],

$$x(t) = 1 - \exp(-Kt^n) \quad (1)$$

where $x(t)$ is the amount of materials transformed at the time (t), K is reaction rate, described by Arrhenius equation and n is Avrami exponent.

The value of n can be calculated by [23],

$$n = \frac{2.5}{\Delta\tau_{\text{FWHM}}} \times \frac{RT_m^2}{E_a} \quad (2)$$

where $\Delta\tau_{\text{FWHM}}$ —full width at half maximum of melting point peak in DSC curve, R —real gas constant, T_m —melting point, and E_a —activation energy. The value of n was calculated from Eq. (2) for different heating rates and presented in Table 2.

Arrhenius equation gives the relation between frequency factor or pre-exponential factor and activation energy.

In chemical kinetic based reactions, Arrhenius equation can be written as [30],

$$K = K_0 \exp\left(\frac{-E_a}{RT}\right) \quad (3)$$

where K is the reaction rate and K_0 is the frequency factor. This equation was used to evaluate the activation energy of the acenaphthene compound. The reaction rate of acenaphthene crystal was evaluated from above equation and the values are presented in Table 2.

Based on JMA theory, Kissingers and Ozawa have developed standard non-isothermal equations for analyzing the activation energy and frequency factor of melting point peak of DSC curve.

The Kissingers [31] and Ozawa [22] equations are given as,

$$\ln\left(\frac{\beta}{T_m^2}\right) = \frac{-E_a}{RT_m} + \ln\left(\frac{K_0 E_a}{R}\right) \quad (4)$$

$$\ln(\beta) = \frac{-E_a}{RT_m} + \ln\left(\frac{K_0 E_a}{R}\right) \quad (5)$$

Kissingers plot was drawn between $\ln(\beta/T_m^2)$ and $1000/T_m$ as shown in Fig. 5. The slope ($-E_a/RT_m$) and intercept of the plot have given the value of activation energy (E_a) and frequency factor (K_0), respectively. The correlation coefficient R -square (R^2) was obtained from Kissingers plot. The values of E_a , K_0 , and R^2 are given in Table 2. In total, $12,940\text{ kJ/mol}$ of activation energy was required to promote the reaction rate of acenaphthene. An estimated frequency factor value $1.6250 \times 10^4\text{ S}^{-1}$ is related to the vibrational frequency of acenaphthene.

Ozawa plot was drawn between $\ln(\beta)$ and $1000/T_m$ as shown in Fig. 6. From the slope the activation energy was

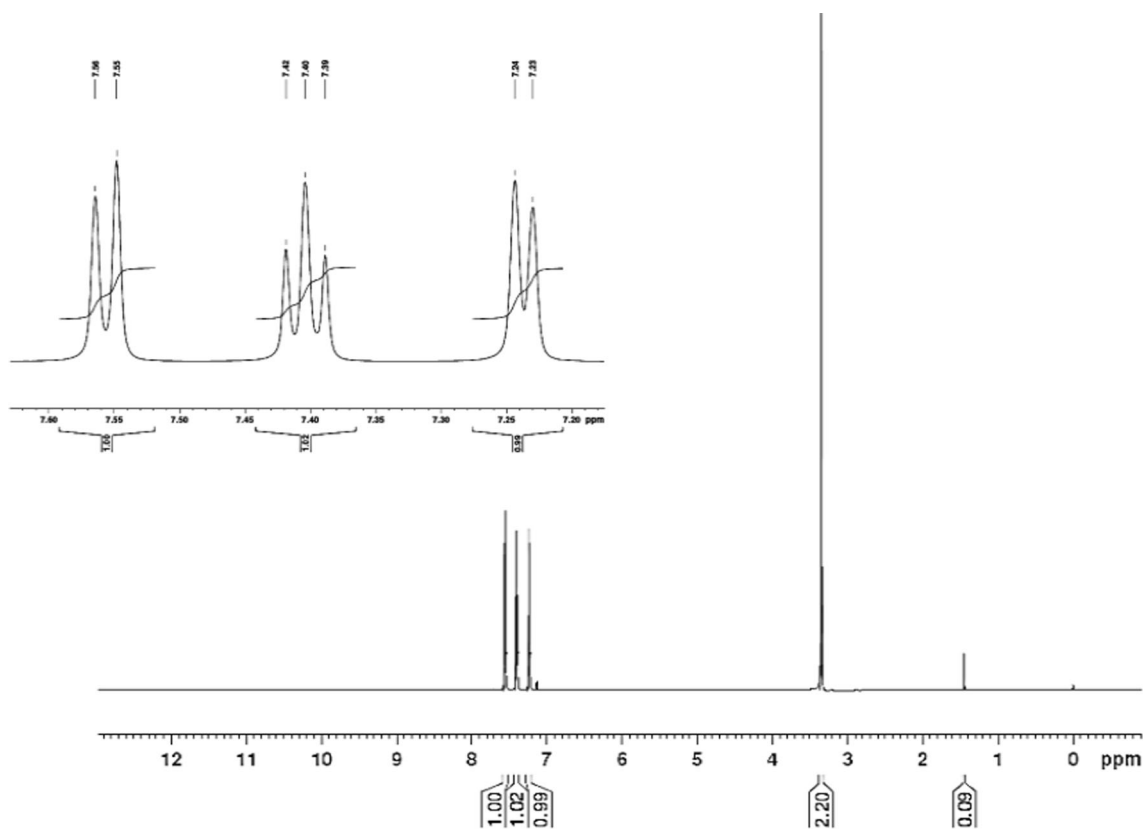


Fig. 3 ^1H NMR of acenaphthene

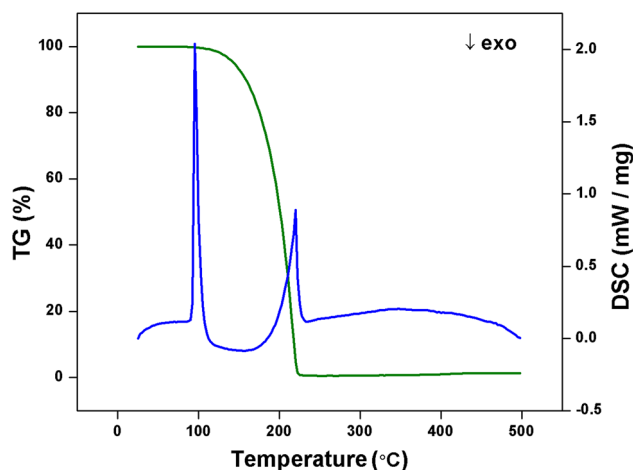


Fig. 4 TG–DSC curves of acenaphthene at heating rate of $10\text{ }^\circ\text{C}$

found to be 14.570 kJ/mol . The calculated activation energy by Kissingers and Ozawa methods for acenaphthene are closer to each other.

The TG curve (Fig. 4) revealed the loss of mass in acenaphthene was started around $130\text{ }^\circ\text{C}$, and single-step decomposition occurred at $245\text{ }^\circ\text{C}$.

The value of degree of conversion was estimated by the relation [24],

$$\alpha = \frac{M_s - M(t, T)}{M_s - M_f} \quad (6)$$

where M_f was the final mass, M_s was the initial mass, and $M(t, T)$ was the instantaneous mass depending on time and temperature. The graph was plotted between calculated α value with temperature (T) as shown in Fig. 7. The value of conversion maximum (α_{max}) for each heating rate was obtained from the first order derivation of plot and the values are given in Table 2. Thermal kinetic parameters of acenaphthene are relatively lower than inorganic materials owing to the low peak temperature (T_m).

3.4 Dielectric constant

In order to determine the dielectric constant, dielectric studies were carried out as a function of frequency at different temperatures.

The dielectric constant (ϵ_r) was calculated by the relation [32],

$$\epsilon_r = Ct/A\epsilon_0 \quad (7)$$

where ϵ_0 is the permittivity of free space, A is the area of cross section of the sample, t is the thickness of the crystal, and C is the capacitance. The variation of dielectric

Table 2 Calculated kinetic parameter values of acenaphthene

Heating rate (β) (°C/min)	T_{max} (°C)	E_a (kJ/mol)	K_0 (S ⁻¹)	K (S ⁻¹)	R^2	n	α_{max} (min ⁻¹)
5	93.59	12.940	1.625×10^4	1.5982	0.95742	2.630	0.02549
10	96.48			1.5990		1.463	0.02787
15	98.37			1.5995		1.724	0.02969
20	100.13			1.5999		1.990	0.03051
25	102.59			1.6005		2.089	0.03114

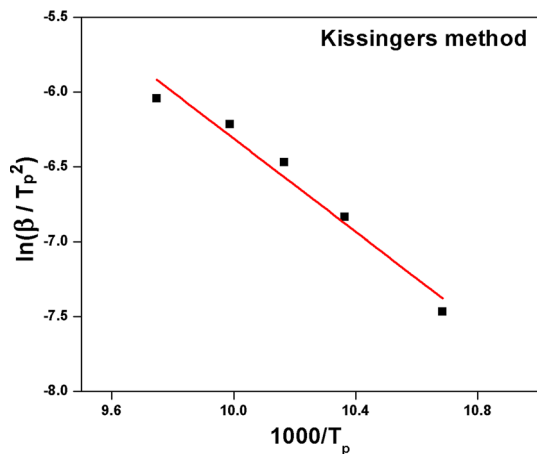


Fig. 5 Plot between $\ln(\beta/T_p^2)$ and $1000/T_p$

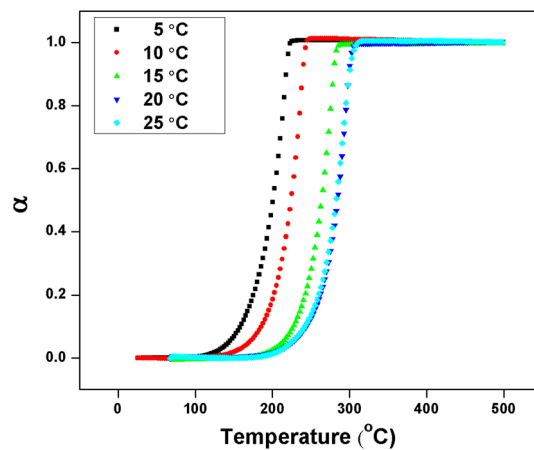


Fig. 7 Plot between α with temperature (T)

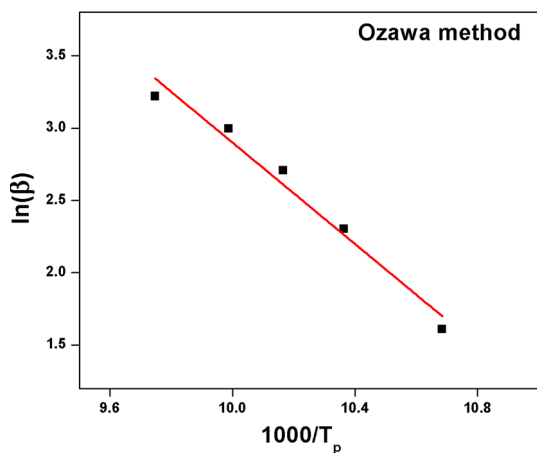


Fig. 6 Plot between $\ln(\beta)$ and $1000/T_p$

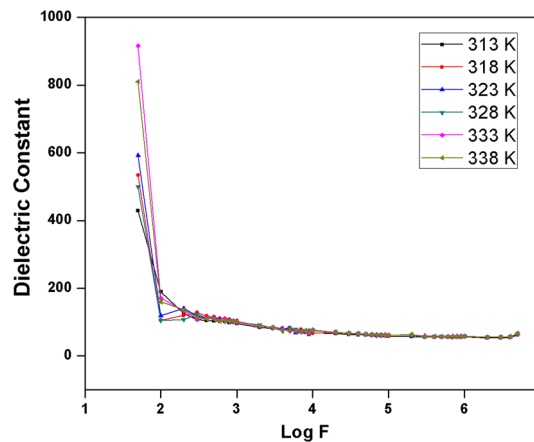


Fig. 8 Variation of dielectric constant with $\text{Log } F$ for acenaphthene crystal

constant (ϵ_r) with different frequencies and temperatures of acenaphthene crystal are shown in Fig. 8. The dielectric constant decreases with higher applied frequency region, whereas at lower frequency region the dielectric constant value was found higher. The charge displacement in crystal and degree of polarization is the leading factors to control the magnitude of dielectric

constant. All the four types of polarizations namely electronic, ionic, orientational, and space charge polarizations are responsible for higher value of dielectric constant at lower frequencies. The ionic and electronic polarizations are strongly independent from temperature and orientational and space charge polarization are temperature dependent.

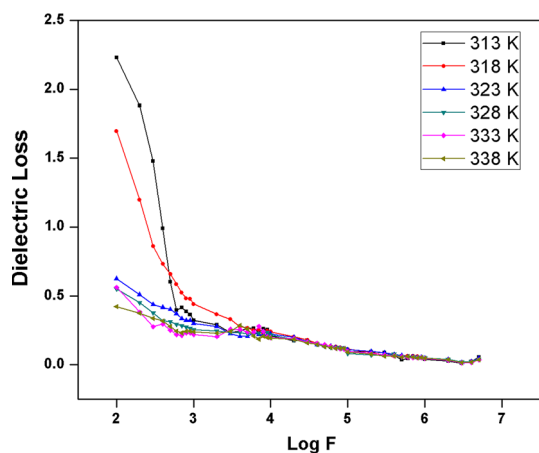


Fig. 9 Variation of dielectric loss with Log *F* for acenaphthene crystal

3.5 Dielectric loss

The dielectric loss factor was directly measured from the impedance analyzer as a function of applied frequencies at different temperatures as shown in Fig. 9. It was clearly inferred that the acenaphthene crystal exhibited very low dielectric loss at high frequencies. It represents the maximum purity of the grown acenaphthene crystal. Similar to that of conduction process, the mechanism of polarization was the basis for the dielectric behavior.

3.6 Electrical conductivity studies

Electrical conductivity provides information of ion transportation and electrons present in crystals. The acenaphthene crystal was subjected to an external electric field to identify the electrical conductivity. While applying the electric field on crystal the current was induced by charge redistribution.

The temperature-dependent AC conductivity of the sample was evaluated by the formula [33, 34],

$$\sigma_{ac} = \epsilon_0 \epsilon_r \omega \tan \delta \tag{8}$$

where ϵ_0 is the absolute permittivity in free space and ω is the angular frequency ($\omega = 2\pi\nu$). The variation in AC conductivity (σ_{ac}) was analyzed with different frequency at different temperature, and it is shown in Fig. 10. The conductivity of crystal was nearly zero in the low-frequency region, and then it increases with increase in frequency. The electronic band structure was changed by decrease in mobility due to ionic size which caused low value of electrical conductivity in the low-frequency region. At higher frequency, all other polarization will not be present except electronic polarization, so in this region conductivity of the material is increased suddenly. Thus the

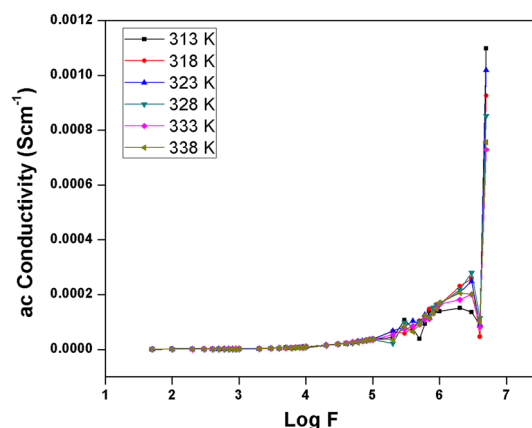


Fig. 10 AC conductivity–frequency dependent plot for acenaphthene crystal

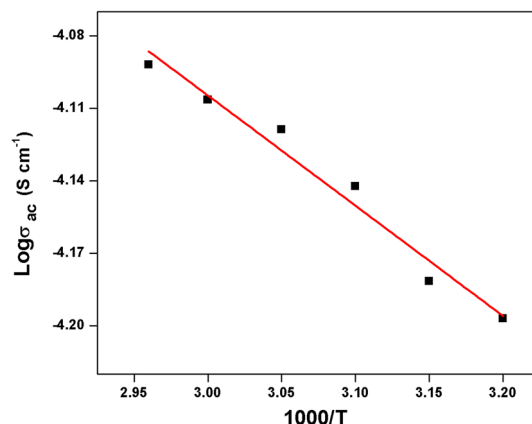


Fig. 11 Arrhenius plot for acenaphthene crystal

conductivity of the grown acenaphthene crystal increases with increase in applied energy.

3.7 Determination of activation energy

The activation energy in terms of electrical performance for acenaphthene crystal was evaluated from Arrhenius plot using the relation [35],

$$\sigma_T = \sigma_0 \exp(-E_a/kT) \tag{9}$$

where σ_T is the electrical conductivity at temperature T , σ_0 is the pre-exponential factor, E_a the activation energy for the electrical conductivity, T is the medium temperature, and k is the Boltzmann constant. From calculated values, the plot was drawn between $\log \sigma_T$ and $1000/T$. The slope of plot (Fig. 11) revealed the average activation energy (E_a) of the acenaphthene crystal, and it was found to be 0.159 eV. The defect present in the crystal affects the charge jumping mechanism, and the activation energy can

cause charge transport from defect position to the next position.

4 Conclusion

The acenaphthene crystal was successfully grown by vertical Bridgman technique by using a single-wall ampoule. Single crystal XRD analysis confirmed the orthorhombic crystal structure of acenaphthene compound with space group $Pcm2_1$. Also the structure of compound was confirmed by 1H NMR analysis. The thermal kinetic parameters of acenaphthene were calculated under non-isothermal condition using TG–DSC measurement. Kissingers method was used to calculate the activation energy (E_a) and frequency factor (K_0) which were found to be 12.940 kJ/mol and $1.625 \times 10^4 S^{-1}$, respectively. Avrami exponent and reaction rate were also calculated at different heating rates. The degree of conversion of acenaphthene crystal was calculated from TG curve. Ozawa method is also used to calculate the activation energy, and it is found to be 14.570 kJ/mol which is close to the value calculated by Kissingers method. The variations of dielectric constant, dielectric loss and AC conductivity of acenaphthene crystal were investigated as a function of frequency at different temperatures. Using Arrhenius equation, the electrical activation energy of the crystal was calculated to be $E_a = 0.159$ eV.

Acknowledgments One of the authors S. Karuppusamy thanks the Anna University authorities for financial support through Anna Centenary Research Fellowship (Lr No: CR/ACRF/JAN2012/36). The authors are thankful to SAIF—IIT Madras for instrumentation facility.

References

1. K. Aravinth, G. Anandha Babu, P. Ramasamy, J. Therm. Anal. Calorim. **1165**, 117 (2014)
2. S.P. Prabhakaran, R. Ramesh Babu, G. Bhagavannarayana, K. Ramamurthi, Bull. Mater. Sci. **151**, 37 (2014)
3. N. Vijayan, G. Bhagavannarayana, N. Balamurugan, R. Ramesh Babu, K.K. Maurya, R. Gopalakrishnan, P. Ramasamy, J. Cryst. Growth **318**, 293 (2006)
4. T. Suthan, N.P. Rajesh, J. Cryst. Growth **3156**, 312 (2010)
5. S. Ayers, M.M. Faktor, D. Marr, D.L. Stevenson, J. Mater. Sci. **31**, 7 (1972)
6. K. Sakata, M. Mukai, G. Rajesh, M. Arivanandhan, Y. Inatomi, T. Ishikawa, Y. Hayakawa, Int. J. Thermophys. **352**, 35 (2014)
7. C.W. Lan, C.Y. Tu, J. Cryst. Growth **406**, 226 (2001)
8. R. Ma, H. Zhang, D.J. Larson Jr, K.C. Mandal, J. Cryst. Growth **216**, 266 (2004)
9. S.T. Balint, L. Braescu, L. Sylla, S. Epure, T. Duffar, J. Cryst. Growth **1564**, 310 (2008)
10. P. Dold, K.W. Benz, Cryst. Res. Technol. **51**, 32 (1997)
11. C.W. Lan, Chem. Eng. Sci. **1437**, 59 (2004)
12. M.G. Kim, G.O. Kim, B.K. Park, KSME Int. J. **1188**, 15 (2001)
13. J.P. Garandet, T. Alboussiere, Prog. Cryst. Growth Charact. Mater. **133**, 38 (1999)
14. D. Morvan, M.E. Ganaoui, P. Bontoux, Int. J. Heat Mass Transf. **573**, 42 (1999)
15. J.R. Cahoon, Can. J. Phys. **140**, 91 (2012)
16. J. Straszko, M. Olszak-Humienik, J. Mozejko, J. Therm. Anal. **1415**, 48 (1997)
17. M. Olszak-Humienik, J. Mozejko, J. Therm. Anal. Calorim. **829**, 56 (1999)
18. S.I. Ali, K. Majid, Thermochim. Acta **183**, 317 (1998)
19. J. Straszko, M. Olszak-Humienik, J. Mozejko, J. Therm. Anal. Calorim. **935**, 59 (2000)
20. S.M. Sidel, F.A. Santos, V.O. Gordo, E. Idalgo, A.A. Monteiro, J.C.S. Moraes, K. Yukimitu, J. Therm. Anal. Calorim. **613**, 106 (2011)
21. E.H. Kissinger, Anal. Chem. **1702**, 29 (1957)
22. T. Ozawa, J. Therm. Anal. Calorim. **301**, 2 (1970)
23. J.A. Augis, J.E. Bennett, J. Therm. Anal. Calorim. **283**, 13 (1978)
24. E. Benavidez, L. Santini, E. Brandaleze, J. Therm. Anal. Calorim. **485**, 103 (2011)
25. R. Ramesh Babu, N. Balamurugan, N. Vijayan, R. Gopalakrishnan, G. Bhagavannarayana, P. Ramasamy, J. Cryst. Growth **649**, 285 (2005)
26. M.A. Lasheen, A.M. Abdeen, Acta Crystallogr. Sect. A. **245**, 28 (1972)
27. R.M. Ribeiro, D.S. dos Santos, R.S. de Biasi, J. Alloys Compd. **227**, 363 (2004)
28. A.A. Joraid, Thermochim. Acta **78**, 436 (2005)
29. R.R. Peláa, L.S. Cividanesa, D.D. Brunellia, S.M. Zanettib, G.P. Thim, Mater. Res. **289**, 11 (2008)
30. S. Lendvayova, K. Moricova, E. Jóna, S. Uherkova, J. Kraxner, V. Pavlík, R. Durny, S.C. Mojumdar, J. Therm. Anal. Calorim. **1133**, 112 (2013)
31. Omer Kaygili, J. Therm. Anal. Calorim. **223**, 117 (2014)
32. P.S. Latha Mageshwaria, R. Priya, S. Krishnan, V. Joseph, S. Jerome Das, Optik **2289**, 125 (2014)
33. B. Uma, Rajnikant, K. Sakthi Murugesan, S. Krishnan, B. Milton Boaz, Prog. Nat. Sci. Mater. Int. **378**, 24 (2014)
34. B. Lal, S.K. Khosa, R. Tickoo, K.K. Bamzai, P.N. Kotru, Mater. Chem. Phys. **158**, 83 (2004)
35. Z. Osman, M.I. Mohd Ghazali, L. Othman, K.B. Md Isa, Results Phys. **1**, 2 (2012)